Electrostatic Characterization of Enzyme Complexes: Evaluation of the Mechanism of Catalysis of Dihydrofolate Reductase

William R. Cannon,* Barbara J. Garrison, and Stephen J. Benkovic*

Contribution from 152 Davey Laboratory, Department of Chemistry, Pennsylvania State University, University Park, Pennsylvania 16802

Received July 29, 1996[⊗]

Abstract: The catalytic mechanism of dihydrofolate reductase is evaluated with Poisson−Boltzmann electrostatic and quantum chemical vibrational frequency calculations. The results indicate that an elevated pK_a of 6.5 associated with the chemical step is due to the formation of the enol tautomer of the substrate's pterin ring. The tautomer is induced to form as a result of substrate binding, in which the substrate desolvates the active site and binds to the carboxylate of Asp 27. Although the binding reaction is favorable, burial of the negative charge on Asp 27 is not. Protonation of Asp 27 occurs, concerted with tautomerization of the substrate, resulting in active site electrical neutrality and activation of the substrate for catalysis. These results require a reinterpretation of previous data from Raman spectroscopy studies in which it was proposed that the reactive atom, the pterin N5, is directly protonated. Quantum chemical vibrational frequency calculations demonstrate that the enol tautomer undergoes a Raman active vibrational perturbation at a frequency similar to that observed experimentally. Furthermore, the calculations indicate that direct protonation of the pterin N5 due to classical electrostatic interactions is quite difficult, with the pK_a for this residue being shifted from 2.6 in solution to below zero while bound to the protein. The conclusions of this work are independent of the protein dielectric constant in the range of 4−20.

Introduction

Dihydrofolate reductase (DHFR) is a ubiquitous enzyme necessary for maintaining intracellular levels of tetrahydrofolate, an active form of the vitamin folic acid, and an essential cofactor in the synthetic pathway of purines, pyrimidines, and several amino acids. DHFR inhibition is the mechanism of action of the antifolate drugs methotrexate and trimethoprin which are used as therapeutic agents in the treatment of various diseases. Because of the medical importance of DHFR and consequently the availability of the enzyme from several sources including cloned, overexpressed protein from bacteria (*Escherichia coli* and *Lactobacillus casei*), fowl (chicken), and mammals (mouse, pig, and human), DHFR provides a convenient model for investigating biological hydride transfer.

The reaction catalyzed by DHFR, shown in Figure 1A, is the reduction of 7,8-dihydrofolate (H_2F) to 5,6,7,8-tetrahydrofolate (H_4F) by the use of the enzyme cofactor nicotinamide adenine dinucleotide phosphate (NADPH; Figure 1C). For the *E. coli* enzyme, the pre-steady-state hydride-transfer rate is pH-dependent and characterized by a pK_a of 6.5 and an optimal rate of 950 s^{-1}.[1] At low pH, H_4F dissociation from the enzyme is rate limiting (12 s^{-1}) for steady-state turnover and occurs after NADPH replaces the oxidized cofactor $NADP^+$ in the ternary complex. At pH > 6.5, reduction of the N5−C6 double bond eventually becomes rate limiting. Furthermore, the kinetic scheme is complicated by the presence of two conformational isomers of the apoenzyme,[2] the relative distribution of which is pH-dependent.[3,4] The conformational degeneracy is also observed in NMR studies of the enzyme−inhibitor complex,[5] and again is pH-dependent.[4] Significantly, binding of the cofactor NADPH results in the presence of only one enzyme conformer.

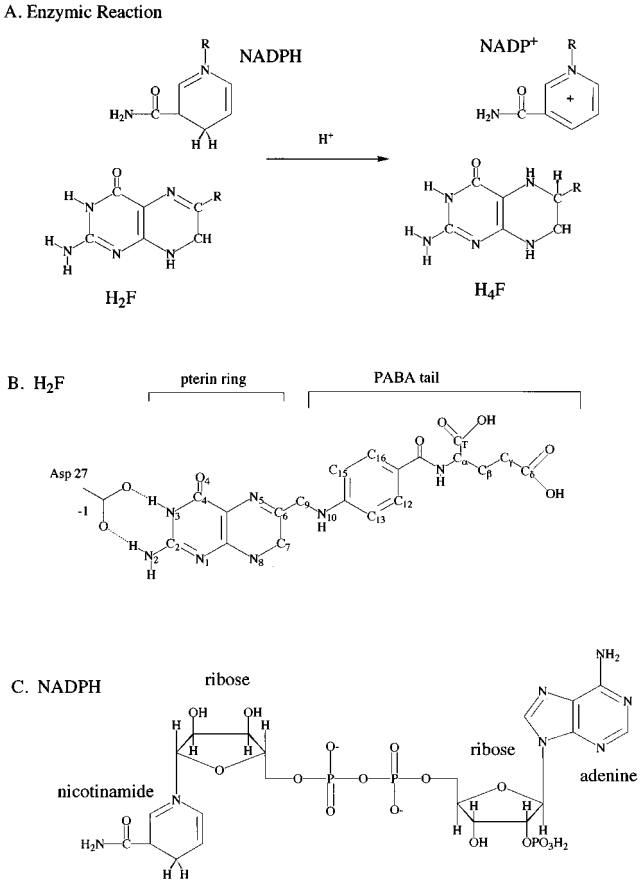

Figure 1. Reaction catalyzed by DHFR and structure of the reactants H_2F and NADPH.

[⊗] Abstract published in *Advance ACS Abstracts,* February 15, 1997.

(1) Fierke, C. A.; Johnson, K. A.; Benkovic, S. J. *Biochemistry* **1987**, *26*, 4085−4092.
(2) Cayley, P. J.; Dunn, M. J.; King, R. W. *Biochemistry* **1981**, *20*, 874−879.
(3) Dunn, S. M.; Lanigan, T. M.; Howell, E. E. *Biochemistry* **1990**, *29*, 8569−8576.
(4) Huang, F. Y.; Yang, Q. X.; Huang, T. H. *FEBS Lett.* **1991**, *289*, 231−234.

S0002-7863(96)02621-2 CCC: $14.00

The availability of three-dimensional structures of the enzyme from X-ray crystallography, beginning in the late 1970s and continuing to the present, has provided the means to integrate the kinetic investigations with structure. Specifically, the crystallographic studies have elucidated the relative orientation of the reactive groups, the pterin ring on H_2F and the nicotinamide ring of NADPH, and also revealed the location of a mechanistically significant residue, Asp 27, which is the only group in the active site capable of providing a proton for the reduction of the H_2F double bond. The Brookhaven protein data base currently contains 29 entries of various structures of DHFR including 10 structures of enzyme−inhibitor or enzyme−inhibitor−cofactor complexes, 6 structures of enzyme−cofactor complexes, 6 structures of enzyme−substrate complexes, 1 structure of the apoenzyme, and 5 structures of nonreactive ternary complexes with substrate or inhibitor. Nevertheless, despite the wealth of information from structure elucidation and the determination of the kinetic schemes for DHFR from several species,[1,6−8] it is not clear how the microscopic events of catalysis proceed, or which features of the enzyme−substrate complex are essential. Although Asp 27 had been implicated in the enzymic reaction because of the pH-dependent nature of the reaction, its mechanism of facilitating proton transfer does not proceed *via* the direct transfer of a proton to N5 of the pterin ring, since the crystallographic studies showed Asp 27 to be in contact with the 2-amino and 3-NH of the pterin, as shown in Figure 1B. As a result, a proton shuffle mechanism was proposed,[9−12] in which Asp 27 provides a proton to be passed through a series of water molecules *via* the pterin O4 to the pterin N5. Recently, Raman spectroscopy revealed that the N5−C6 bond on H_2F undergoes a measurable vibrational perturbation at pH 6.5,[13] which is the same pH at which the catalytic hydride-transfer step is maximal.[1] This observation was interpreted as evidence for direct protonation of N5, without involvement of Asp 27. The N5 site of the pterin ring, however, has a pK_a of 2.6 in solution, and no structural explanation for the apparent large shift in pK_a could be provided. The vibrational perturbation was only observed for the ternary DHFR·$NADP^+$·H_2F complex, and not the binary DHFR·H_2F complex.

In this paper, we report the results of Poisson−Boltzmann calculations[14−16] which were used to characterize the electrostatic properties of the binary enzyme−cofactor complex and two complexes of the ternary enzyme−cofactor−substrate which differ by the tautomeric state of the bound substrate. Structures used in the calculations were from crystallographic studies, or were closely modeled after the crystallographic coordinates in the case of the ternary enzyme complex.

The electrostatic nature of the complexes suggests a mechanism of hydride transfer which differs from previous proposals based on interpretation of experimental titration curves, structure, or Raman spectroscopy, yet the suggested mechanism is consistent with the experimental data obtained in these studies and others. Conclusions drawn from the electrostatic calculations concerning the catalytic mechanism are supported by *ab initio* electronic structure calculations.

Additionally, the electrostatic calculations implicate a weak base, His 45, as being important for cofactor binding. Examination of DHFR sequences from 40 other species indicates that this residue is indeed functionally significant, as weak bases are found in 75% of the sequences at the analogous position. It is suggested that this residue is responsible for the pH-dependent nature of the enzyme conformational equilibria involved in binding ligands.

Methods

Electrostatic Calculations. Calculation of pK_a values was done using the method of Antosiewicz et al.[16] The pK_a values for amino acid groups in solution, as determined by experiment, were used as model pK_a values and the starting points of the calculations. The linearized Poisson−Boltzmann equation was then used to determine pK_a values for the same groups in the enzyme environment. The enzyme was modeled as a low dielectric medium ($\epsilon = 20$) comprised of point charges representing the partial charges of atoms. The Richards solvent accessible surface was used to determine the extent of the enzyme environment.[17] The solvent was modeled as a high-dielectric medium ($\epsilon = 80$) and characterized by an ionic strength of 150 mM. The final pK_a value is determined by turning on interactions between ionizable residues in their charged states and determining the lowest energy ionization state of the structure using the method of clustering ionizable groups.[18]

For amino acids, the model dissociation acid constants, pK_a^{model}, are the dissociation constant values for each amino acid side chain in solution.[19,20] Model values for groups on H_2F and NADPH are from various sources. For instance, the model acid dissociation constants for the pyrophosphate bridge are from experimental data for thiamine pyrophosphate.[21] The model pK_a for secondary ionization of this group is identical in value to that for the primary ionization (1.3), because the observed secondary ionization (∼6.6) results in large part from the electrostatic influence of the primary ionization; thus, using the experimentally observed value for secondary ionization would overaccount for this effect.[22] The acid dissociation values for the primary ionization of the 2′-ribose phosphate group of NADPH was not determined as further development of the method would be required. As the primary ionization occurs below pH 1, however, the effect of this group on titrations occurring near physiological pH will be negligible.

Structures for the DHFR·NADPH holoenzyme and the DHFR·$NADP^+$·folate ternary complex were obtained from the Protein Data Bank files 1drh and 7dfr,[12a] respectively. Polar hydrogens were added using the CHARMm[23] molecular modeling package, except for aspartic acid, glutamic acid, and histidine residues which were added manually. Ten hydrophilic residues are incomplete in the ternary structure and were built using the Quanta/CHARMm molecular editor.[23] These residues were located on the surface of the protein.

The geometries of the ligands were taken from the respective crystallographic data files, except for the bond geometries of the nicotinamide ring of NADPH and the pterin ring of H_2F. These groups were optimized by quantum chemical Hartree−Fock calculations

(5) Falzone, C. J.; Wright, P. E.; Benkovic, S. J. *Biochemistry* **1991**, *30*, 2184−2191.
(6) Andrews, J.; Fierke, C. A.; Birdsall, B.; Ostler, G.; Feeney, J.; Roberts, G. C. K.; Benkovic, S. J. *Biochemistry* **1989**, *28*, 5743−5750.
(7) Appleman, J. R.; Beard, W. A.; Delcamp, T. J.; Prendergast, N. J.; Freisheim, J. H.; Blakely, R. L. *J. Biol. Chem.* **1990**, *265*, 2740−2748.
(8) Thillet, J.; Adams, J. A.; Benkovic, S. J. *Biochemistry* **1990**, *29*, 5195−5202.
(9) Gready, J. *Biochemistry* **1985**, *24*, 4761−4766.
(10) Morrison, J. F.; Stone, S. R. *Biochemistry* **1988**, *27*, 5499−5506.
(11) Uchimaru, T.; Tsuzuki, S.; Tanabe, K.; Benkovic, S. J.; Furukawa, K.; Taira, K. *Biochem. Biophys. Res. Commun.* **1989**, *161*, 64−68.
(12) (a) Bystroff, C.; Oatley, S. J.; Kraut, J. *Biochemistry* **1990**, *29*, 3263−3277. (b) McTigue, C.; Davies, J. F.; Kaufman, B. T.; Kraut, J. *Biochemistry* **1992**, *31*, 7264−7273. (c) Reyes, V. M.; Sawaya, M. R.; Brown, K. A.; Kraut, J. *Biochemistry* **1995**, *34*, 2710−2723.
(13) Chen, Y. Q.; Kraut, J.; Blakely, R. L.; Callender, R. *Biochemistry* **1994**, *33*, 7021−7026.
(14) Honig, B.; Nicholls, A. *Science* **1995**, *268*, 1144−1149.
(15) Bashford, D.; Karplus, M. *Biochemistry* **1990**, *29*, 10219−10225.
(16) Antosiewicz, J.; McCammon, J. A.; Gilson, M. K. *J. Mol. Biol.* **1994**, *238*, 415−436.
(17) Richards, F. M. *Annu. Rev. Biophys. Bioeng.* **1977**, *6*, 151−176.
(18) Gilson, M. K. *Proteins: Struct., Funct., Genet.* **1993**, *15*, 266−282.
(19) Stryer, L. *Biochemistry*, 2nd ed.; W. H. Freeman and Co.: New York, 1981.
(20) Nozaki, Y.; Tanford, C. *Methods Enzymol.* **1967**, *11*, 715−734.
(21) Lachmann, H.; Schnackerz, K. D. *Org. Magn. Reson.* **1984**, *22*, 101−105.
(22) Potter, M. J.; Gilson, M. K.; McCammon, J. A. *J. Am. Chem. Soc.* **1994**, *116*, 10298−10299.
(23) Molecular Simulations, Inc., San Diego, CA.

Table 1. Comparison of the Charges Used for the 4-Oxopterin and Nicotinamide Rings in the Electrostatics Calculation (Derived from HF/3-21G) and Similar Charges from a HF/6-31G(d) Calculation

4-oxo pterin			nicotinamide ring			
atom	3-21G	6-31G(d)	atom	PB calcd	3-21G	6-31G(d)
N1	−0.894	−0.934	N1	−0.05	−0.041	−0.103
C2	1.156	1.233	C2	−0.05	−0.051	0.024
N2	−1.076	−1.172	H2	0.15	0.161	0.126
H2a	0.415	0.474	C3	−0.15	−0.296	−0.380
H2b	0.493	0.483	C4	0.20	0.225	0.609
N3	−0.891	−0.941	H4a	0.025	0.028	−0.094
H3	0.423	0.444	H4b	0.025	−0.005	−0.119
C4	0.780	0.824	C5	−0.30	−0.316	−0.392
O4	−0.624	−0.648	H5	0.15	0.142	0.120
C4a	0.016	−0.177	C6	−0.15	−0.147	−0.062
N5	−0.689	−0.574	H6	0.15	0.172	0.134
C6	0.549	0.365	C7	0.55	0.869	0.895
C7	−0.010	0.223	O7	−0.55	−0.665	−0.698
H7a	−0.038	−0.011	N7	−0.60	−1.048	−1.052
H7b	−0.047	−0.064	H7	0.30	0.444	0.442
N8	−0.214	−0.541	H7	0.30	0.415	0.418
H8	0.310	0.356				
C8a	0.341	0.591				

Table 2. Model and Calculated pK_a Values for NADPH and H_2F

	NADPH			H_2F			
structure	ADN	2′-PO_3	$-P_2O_7H_2-$	C4−N3	N5	CD	CX
model	3.8[52]	6.8	1.0/1.0[21]	10.8[53]	2.5[53]	4.7[54]	3.4[54]
holoenzyme	1.8	6.3	−0.3/−3.2				
enol pterin	1.8	6.4	−0.6/−1.4	17.5	−1.4	4.8	0.4
keto pterin	1.8	6.4	−0.6/−1.5	17.5	−0.8	4.9	0.4

employing the Gaussian92 program[24] and the 3-21G basis set, using the initial geometries of the oxidized nicotinamide ring of $NADP^+$ and the pterin ring of folate from the crystallographic data files. The DHFR·NADPH·H_2F model was then constructed from the crystallographically determined structure of the DHFR·$NADP^+$·folate complex by incorporating the bonded geometry of the reduced nicotinamide ring and H_2F from the quantum chemical calculations. Both the 4-oxo (keto) and 4-hydroxy (enol) forms of the pterin ring were employed in separate calculations.

The potential parameters used were those used in the original method, with the exception of H_2F and NADPH partial charges. CHARMm v.22 partial charges along with OPLS Lennard-Jones parameters were used for all amino acid residues. Partial charges for the pterin and benzoyl rings of H_2F were obtained from the quantum chemical calculations, in which the electrostatic fields were fit to point charge models by a least squares optimization using the CHELPG algorithm.[25] The partial charges were modified insignificantly so that the sum of partial charges is zero on each of the pterin ring and the PABA tail. Charges for the α-carboxyglutamate tail of H_2F were taken from standard CHARMm v.22 charges for glutamic acid. A similar procedure was carried out for NADPH; however, in order to make the HF/3-21G CHELPG charges on the nicotinamide ring sum to zero, a slightly greater modification was made. In order to maintain consistency, the charges used for the carboxamide group of the nicotinamide ring were standard charges from the CHARMm v.22 parameter set for carboxamide groups. A comparison of the HF/3-21G charges, the actual charges used in the calculations, and those determined by a single-point HF/6-31G(d) calculation with CHELPG fitting is shown in Table 1 for the 4-oxopterin ring and the nicotinamide ring.

Lennard-Jones parameters for the ligand atoms were adopted from similar OPLS atom types. These parameters were not optimized for general use but are available as Supporting Information. (Use of the charge parameters for molecular mechanics simulations would require further development. Although the charges obtained in this manner provide a good representation of the surrounding electrostatic field for the particular configuration of the ligands found in the crystallographic structure, no attempt has been made to optimize the charges with respect to different ligand conformations; furthermore, the charges, atomic radii, and dispersion energies must be appropriately matched for use in molecular mechanics simulations.)

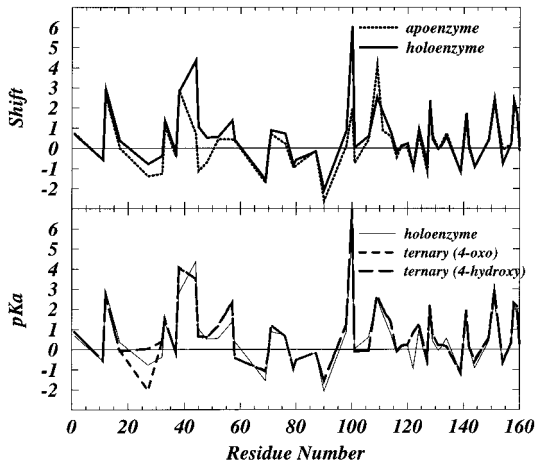

Figure 2. Comparison of calculated pK_a shifts for protein residues of (A, top) the apoenzyme and holoenzyme and (B, bottom) the holoenzyme and model reactive ternary complexes of DHFR.

Vibrational Frequency Calculations. For comparison with experimental vibrational spectroscopy data, the normal mode vibrations of six dihydrofolate complexes with acetic acid or acetate ion were examined as shown in Figure 6. The geometries of these structures were fully optimized at the Hartree−Fock level of theory employing the 3-21G and 6-31G basis sets. Stationary points on the potential energy surface were characterized by convergence of energy and geometry to within predetermined values, while normal mode vibrational frequency calculations were used to determine that the stationary points were minima by the absence of imaginary frequencies. Raman and IR absorbances were determined from the normal mode analysis and overlap integrals of the polarizability and dipole moment, respectively.

Results

Determination of pK_a Values. The results are discussed in the context of the calculated pK_a and the intrinsic pK_a. While the former value is comparable to experiment, the intrinsic pK_a does not include the effect of charge−charge interactions due to titrations of other groups and represents the pK_a when only desolvation and dipole−dipole interactions are taken into account in an otherwise neutral protein. In general, the greatest pK_a shifts are seen for desolvated groups in the interior of the protein.

Results for the determination of pK_a values by Poisson−Boltzmann calculations are summarized in Figure 2, in which the pK_a shift relative to the pK_a of the group in solution is plotted against the residue number. (The pK_a values of all protein residues are available as Supporting Information in tabular form.) First, we examine the effect of cofactor binding on the enzyme by comparing the titration behavior of the holoenzyme with that of the previously determined apoenzyme.[26] Next, we evaluate the influence of substrate binding to the holoenzyme by comparing results for the holoenzyme with those of the two ternary complexes. In the active site, the titration behavior of the three complexes differs especially at Asp 27, which we examine in detail. Residues removed from the active site but still influential on binding and catalysis are considered next. Finally, we present the results from quantum chemical vibra-

(24) Frisch, M.; Head-Gordon, M.; Trucks, G.; Foresman, J.; Schlegel, H.; Raghavachari, K.; Robb, M.; Binkley, J.; Gonzalez, C.; Defrees, D.; Fox, D.; Whiteside, R.; Seeger, R.; Melius, C.; Baker, J.; Martin, R.; Kahn, L.; Stewart, J.; Topiol, S.; Pople, J., Gaussian, Inc., Pittsburgh, PA, 1992.

(25) Breneman, C.; Wiberg, K. *J. Comput. Chem.* **1990**, *11*, 361−373.

(26) Cannon, W. R.; Garrison, B. J.; Benkovic, S. J. Manuscript in preparation.

tional frequency calculations, which are compared with experimental observations from Raman spectroscopy of a ternary DHFR complex.

Effect of Cofactor Binding on Active Site Residues. Figure 2A compares the pK_a shifts for the holoenzyme with those for the apoenzyme. The features of the two plots are generally similar but have noticeable differences at several titratable sites. As the crystal structure for the apoenzyme is missing loop 1 (residues 16−20), the calculated pK_a shift for Glu 17 appears as 0.0, while for the holoenzyme this residue is shifted up from its solution value by 0.4.

In both structures, Asp 27 is shifted below its solution value of 4.0, and the perturbation appears slightly stronger in the apoenzyme than in the holoenzyme. As loop 1 closes over the active site pocket in which Asp 27 is located, it may partially desolvate the pocket. Thus, there may not be any actual difference in the titration behavior of Asp 27 in the two structures.

Tyr 100 binds to NADPH at the nicotinamide C4. The binding involves interaction between the Tyr O_η and the nonreactive hydrogen attached to the nicotinamide C4, with a distance of 3.1 Å between O_η and C4. A significant upward spike occurs at this location for the holoenzyme shown in Figure 2A. In the apoenzyme structure this residue is solvent exposed, and the large pK_a shift seen here for the holoenzyme is due to both desolvation and charge−charge interactions. The intrinsic pK_a accounts for about 46% of the observed shift in the holoenzyme, while a further upward shift in pK_a results when interactions with charged states of other ionizable groups are taken into account, indicating that Tyr 100 must lie in a region of negative electrostatic potential. The doubly charged diphosphate bridge of NADPH and the carboxylate of Asp 27 both lie approximately 8.5 Å away from the Tyr η-oxygen, and the carboxylate of Glu 101 lies approximately 11 Å away. In the low-dielectric interior of the protein, the potentials due to these charges are unmitigated by complementary fields which could be generated by weak bases. As the adjoining hydrogen on the nicotinamide C4 is the hydride that is transferred during catalysis, Tyr 100 can be expected to affect the catalytic rate. Indeed, a 10-fold drop in hydride transfer rate occurs when the terminal hydroxyl group on the Tyr 100 side chain is removed by interchanging this residue with isoleucine, corresponding to a 1.4 kcal mol^{-1} increase in activation energy.[27]

Binding of the Nonreactive Moieties of NADPH. The nonreactive tail of NADPH consists of two riboses connected by a diphosphate bridge, and an adenine ring extending from the second ribose, as shown in Figure 1C. These groups provide noncovalent interaction sites with the protein and are important in positioning the cofactor for catalysis. The protein residues Arg 44 and His 45 bind NADPH as shown in Figure 3, and as a result, the titration behavior of these residues differs significantly between the holoenzyme and apoenzyme. Arg 44 is less than 2.5 Å from the charged 2′-ribose phosphate moiety of NADPH, and His 45 is close to the diphosphate bridge of NADPH. Both of these groups are solvent exposed in the apoenzyme structure. In comparison, Arg 98 also is in contact with the 2′-ribose phosphate and the adenine base of NADPH, but shows only a small change in titration behavior compared to the apoenzyme.

As would be expected, the phosphate groups on the NADPH cofactor are also perturbed somewhat by binding, as shown in Table 2. The 2′-ribose phosphate group is slightly shifted down from its solution value, and both phosphate groups of the diphosphate bridge are similarly affected. ^{31}P-NMR solution studies of enzyme−cofactor complexes from both *L. casei*[29] and *E. coli*[30] indicate that the 2′-ribose phosphate group is in its dianionic form throughout the pH range of 5−7; however, solid state ^{31}P-NMR studies of lyopholized *L. casei* DHFR·NADPH and DHFR·NADP$^+$ complexes indicte that both dianionic and monoanionic forms of the 2′-ribose phosphate exist between pH values of 6.0 and 6.5.[31] The calculated pK_a of 6.3 for the 2′-ribose phosphate may be an indicator that the crystalline environment on which the calculations are based may have more similarity to the lyopholized protein complex than the protein complex in solution, at least for this group.

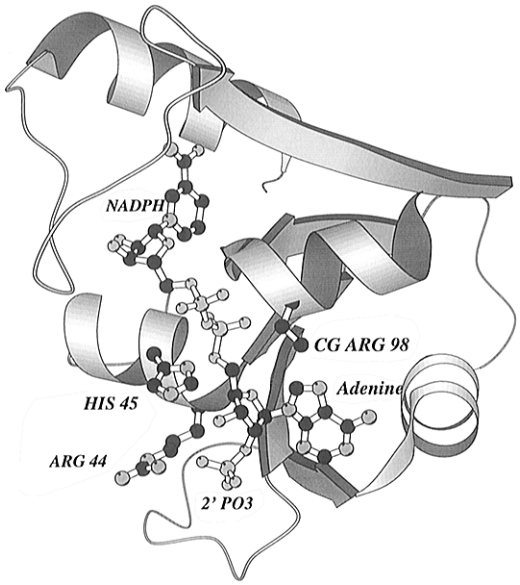

Figure 3. Structure of the NADPH binding site showing protein and cofactor groups important in binding. Only part of the Arg 98 side chain is shown for clarity. The graphics were made with Molscript.[28]

The adenine base of NADPH is both removed from solvent and in close contact with protonated Arg 98 as shown in Figure 3, resulting in a pK_a shift of nearly 2 units from its solution value. As shown in Table 2, these trends for NADPH titration are also followed in the structures for the ternary DHFR·NADPH·H_2F complex.

Ternary Enzyme Complexes: Effect of Substrate Binding. In Figure 2B the titration behavior of the ternary complex is compared with that of the holoenzyme. Both the 4-oxo (keto) and 4-hydroxy (enol) forms of the pterin ring of dihydrofolate were employed in two separate calculations, and their behavior is also compared in Figure 2B. The most striking difference in the titration of the three structures is that of Asp 27. The ternary structure employing the 4-hydroxypterin shows Asp 27 to be shifted 2.2 pK_a units more positive than in the same structure for the 4-oxopterin. The holoenzyme pK_a is intermediate between these two. As this residue is involved in catalysis and its proposed role has been a point of controversy, we examined the titration behavior of this residue in detail.

The structure of the active site as it exists in the holoenzyme is shown in Figure 4A, in which Asp 27 is located in a hydrated pocket of the protein with three crystallographic waters within 3.6 Å and an additional two waters within 4.3 Å. Upon binding

(27) Adams, J. A.; Fierke, C. A.; Benkovic, S. J. *Biochemistry* **1991**, *30*, 11046−11054.
(28) Kraulis, P. J. *J. Appl. Crystallogr.* **1991**, *24*, 946−950.
(29) Feeney, J.; Birdsall, B.; Roberts, G.; Burgen, A. *Nature* **1975**, *257*, 564−566.
(30) Cayley, P. J.; Feeney, J.; Kimber, B. J. *Int. J. Biol. Macromol.* **1980**, *2*, 251−255.
(31) Gerothanassis, I. P.; Barrie, P. J.; Birdsall, B.; Feeney, J. *Eur. J. Biochem.* **1994**, *226*, 211−218.

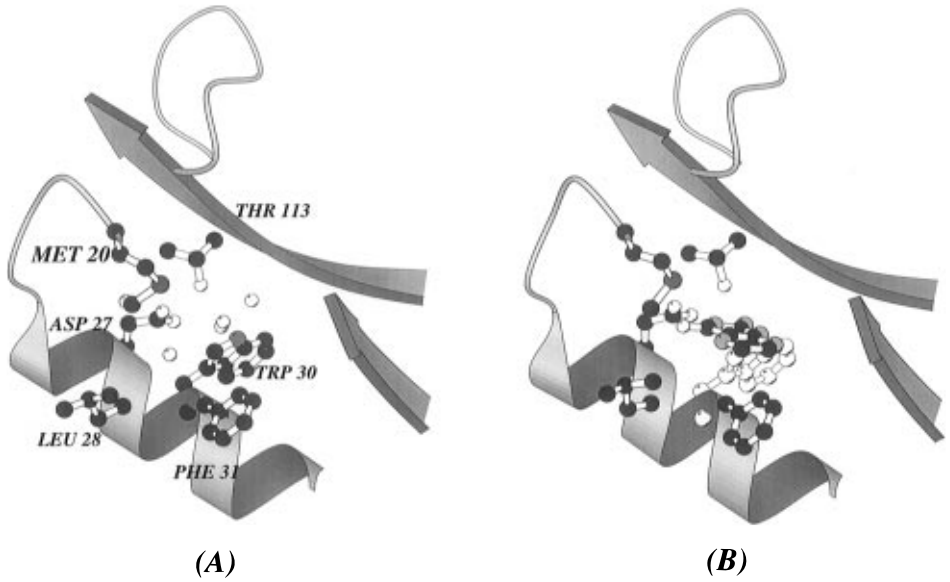

Figure 4. Active site structure of (A) the holoenzyme in which the five nearby waters are shown as unfilled circles and (B) the ternary complex in which substrate displaces water (Trp 22 shown as unfilled circles for clarity). The graphics were made with Molscript.[28]

of substrate, these waters are displaced by the substrate's pterin ring, as shown in Figure 4B. In the holoenzyme structure, as in the structures of both ternary complexes, the local dipole interaction from the protein consists of hydrogen bonding between the side chain hydroxyl group of Thr 113 and the carboxyl of Asp 27.

It has been suggested that in special cases the pK_a of a group which is partially desolvated may be underestimated by this method, owing to the relatively high dielectric constant employed for the protein interior ($\epsilon = 20$).[16] Although the dielectric response of the protein interior is probably more accurately described by a dielectric constant of 4, a value of 20 has been empirically observed to yield the most accurate results, likely by indirectly accounting for the conformational flexibility of titrating groups on the protein, nearly all of which are located on the protein surface. The availability of alternative conformations for groups upon titration can moderate the size of a shift in pK_a. In this regard it has been shown that using a dielectric constant of 4 for the protein interior and directly examining different protein conformational states leads to improved results over pK_a values obtained when a dielectric of 4 and a static structure are used.[32] Enzyme and substrate groups located in the active site, however, are unlikely to have much conformational freedom.[33] In this case, the use of a dielectric constant of 4 may be most appropriate.

As a consequence we examined the titration behavior of Asp 27 as a function of the protein dielectric constant employed in the calculations. The results are shown in Figure 5, in which the bold lines indicate the calculated pK_a and the light lines indicate the intrinsic pK_a. (Results for other groups are available as Supporting Information.) For the holoenzyme and the ternary complex with the 4-hydroxy tautomer of the pterin ring, both the calculated pK_a and the intrinsic pK_a increase with a decreasing dielectric response of the protein environment. The effect is markedly greater, however, for the ternary complex with the 4-hydroxypterin. This is expected, as four of the crystal waters in the holoenzyme structure, shown in Figure 4A, are displaced by binding of the substrate in the ternary complex (Figure 4B), further reducing the dielectric response of the local environment. Moreover, tautomerization of the 4-oxopterin,

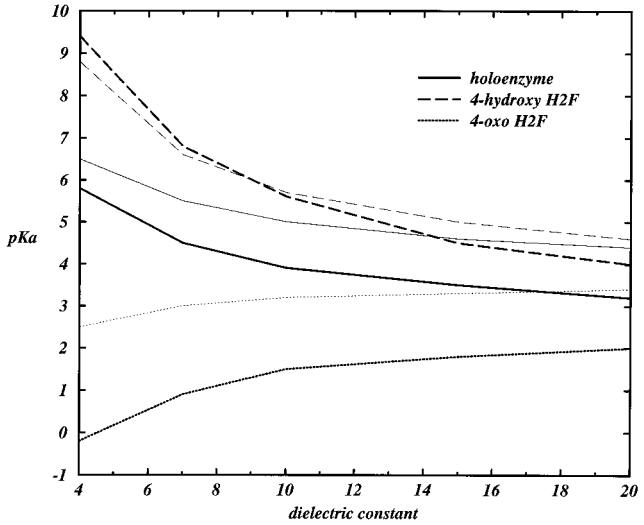

Figure 5. Titration behavior of Asp 27 as a function of the protein dielectric value for the holoenzyme and both ternary complexes, in which the bold line is the pK_a and the light line indicates the intrinsic pK_a.

shown in Figure 1B, to the 4-hydroxypterin results in an unfavorable charge−dipole interaction between $O_{\delta 2}$ of Asp 27 and N3 of the pterin ring, which bears a partial charge of −0.96 obtained from the quantum mechanical calculations.

In contrast, both the calculated pK_a and the intrinsic pK_a decrease for the ternary complex containing the 4-oxo tautomer of the pterin ring as the dielectric response decreases. In this structure all local dipolar interactions are favorable for the ionized Asp carboxyl group: one carboxyl oxygen ($O_{\delta 1}$) binds to the N2 amine group of the pterin ring as in the 4-hydroxypterin structure, while the other carboxyl oxygen ($O_{\delta 2}$) binds to the amide N−H dipole at N3 as shown in Figure 1B. The Thr 113 side chain hydroxyl accounts for a third favorable dipole−charge interaction at this site.

From these observations it is apparent that involvement of Asp 27 in a catalytic event characterized by a pK_a of 6.5[1] is more likely to be associated with the 4-hydroxy rather than 4-oxo tautomer of the pterin ring of the substrate.

Nevertheless, the observed catalytic dependence on a titratable group with a pK_a of 6.5 may also be due to groups on the

(32) You, T. J.; Bashford, D. *Biophys. J.* **1995**, *69*, 1721−1733.
(33) Cannon, W. R.; Singleton, S. F.; Benkovic, S. J. *Nature Struct. Biol.* **1996**, *3*, 821−833.

substrate, particularly the pterin N5 which lies 5.7 Å from Asp 27. As shown in Table 2, however, the calculations indicate that the pK_a of this group for both ternary complexes is shifted markedly downward from the solution value of 2.5 to below zero. Nearly the entire pK_a shift determined by the calculations is attributed to the transfer of this group from solution into the hydrophobic active site pocket due to the difficulty of charging the group in the low-dielectric environment.

Remote Effects on the Active Site. Although Asp 122 is not part of the nominal active site, in both the holoenzyme and the ternary complex, the Asp 122 side chain interacts with the backbone carbonyl and amino groups of Glu 17 and Asn 18. These two amino acids constitute part of a five-residue loop that folds over the active site. In the ternary complex, unfavorable electrostatic interactions are seen. The Glu 17 backbone carbonyl dipole is directed toward the carboxyl group of Asp 122, while the amino N−H dipole is directed away from the same carboxyl group, resulting in an upward shift in the pK_a of Asp 122 relative to the free amino acid in solution.

In the holoenzyme structure, however, there is a conformational change in the backbone ϕ and ψ angles of Glu 17, resulting in favorable interactions to the carboxyl side chain of Asp 122. Both of the backbone amide N−H dipoles of Glu 17 and Asn 18 are directed toward the carboxyl side chain of Asp 122 and form hydrogen bonds to the carboxyl oxygens. Likewise, the backbone carbonyl of Glu 17 is directed away from Asp 122.

The result of the different configurations seen in the holoenzyme and the ternary complex is a shift in the pK_a of Asp 122 by nearly 2 pH units between the structures. Previous work has implicated these groups as being conformationally and dynamically important for catalysis. Residues 16−20 undergo a loop-opening process on the millisecond time scale,[34] and removal of the loop results in a 560-fold decrease in k_{cat}.[35] The effective relaxation times for local structural fluctuations of the backbone amine groups of residues around Glu 17 are in the range 80−4000 ps from NMR studies.[36] Interestingly, substitution of the neighboring Gly 121, which undergoes relatively large motions on the nanosecond time scale,[36] for valine or leucine, which are likely to be more conformationally restrained, results in 240- and 52-fold decreases in k_{cat}.[37]

Binding of the PABA Tail of the Substrate. Lys 32 and Arg 52 and 57 bind the carboxyl groups of the PABA tail of the substrate, and as a consequence the pK_a values of these groups are shifted upward in the substrate bound structures. These three residues form an ionic cluster on the surface of the protein with the two carboxyl groups of the PABA tail of H_2F and have previously been implicated by electrostatic calculations as being significant for substrate binding.[38] The results shown in Table 2 parallel those in the study of methotrexate binding to DHFR.[26]

Ionic Clustering on the Enzyme Surface. The architecture of the DHFR fold results in a complex clustering of titratable groups on the surface of the enzyme that includes Lys 38 and 109. Lys 109 exhibits unique shifts between the apo- and holoenzyme structures, with the apoenzyme being perturbed to a greater degree. Binding of substrate does not appear to affect the pK_a of Lys 109 further. Both calculations result in a similar intrinsic pK_a, 10.5 for the apoenzyme and 10.3 for the holoenzyme. The increased pK_a for Lys 109 in the apoenzyme with respect to the holoenzyme suggests that there is a stronger electronegative field in the vicinity of Lys 109 in the apoenzyme.

In contrast, the calculated pK_a of Lys 38 is unaffected by binding of NADPH, yet is shifted about 1 pH unit higher in the ternary complex than in the holoenzyme. The precise cause of the pK_a shift relative to the holoenzyme was not determined.

Vibrational Frequency Calculations. The total energies and frequencies corresponding to the N5−C6 stretch for six dihydrofolate−acetic acid/acetate ion complexes were examined. These complexes serve as models for characterizing various states of the bound substrate, which can be compared to the results from Raman spectroscopy studies on DHFR complexes.[13] Before comparing vibrational frequencies observed in the Raman study with those reported here, however, it is important to understand how they differ. Frequencies derived from electronic structure calculations are known to be 10−15% higher than their counterparts from experimental data due to the effects of electron correlation,[39] which are not taken into account in the calculation. Furthermore, the differences between experimental and calculated frequencies are systematically reduced when harmonic frequencies from experiment can be compared with the calculated normal mode frequencies.[39] Nevertheless, the trend within the series of frequencies which can be observed experimentally is well replicated by electronic structure calculations.[39] Figure 6 shows the structures of the various active site models along with the relative energies, the frequency of the N5−C6 stretch, and the normal mode of this vibration, in which the normal mode vibrational displacements are overlayed on the atomic structure of the complex and are identifiable as pink atoms.

The neutral pterin that exists in solution is the 4-oxo-7,8-dihydro configuration,[40] which serves as a reference for comparisons (Figure 6, **1**). Acetate serves as a model for the Asp 27 carboxylate which binds to the pterin ring as shown. The frequency of the N5−C6 stretch is 1893 cm^{-1} and differs from the Raman observed frequency of 1650 cm^{-1} in the enzyme ternary complex by 12.9%, which is in accord with comparisons of other calculated and experimental frequencies.[39] Although many atoms other than N5 and C6 are involved in the normal mode vibration, it consists predominately of the N5−C6 stretch as demonstrated by the normal mode displacement coordinates.

Tautomerization of the pterin ring along with protonation of Asp 27 leads to the 2-amino-4-hydroxy structure **2** shown in Figure 6. The frequency of the N5−C6 stretch for this species is 15 cm^{-1} greater than that for the 4-oxopterin. As **1** differs from this structure and all other structures in Figure 6 by a proton, comparison of relative energies is not possible. A second 4-hydroxy tautomer (**3**) involving an N2-imine can be formed as shown in Figure 6; however, this structure is less stable relative to **2** by 13 kcal mol^{-1}.

Three structures (**4**−**6**) involving protonation at N5 can be constructed as shown, where **4** is the structure of the N5-protonated 4-oxopterin complexed to the model Asp 27 carboxylate group. The N5−C6 normal mode stretch for **4** occurs at a frequency 8 cm^{-1} greater than that for **1**, and the hydrogen attached to N5 is also active in this vibration. The normal mode

(34) Falzone, C. J.; Wright, P. E.; Benkovic, S. J. *Biochemistry* **1994**, *33*, 439−442.
(35) Li, L.; Falzone, C. J.; Wright, P. E.; Benkovic, S. J. *Biochemistry* **1992**, *31*, 7826−7833.
(36) Epstein, D. M.; Wright, P. E.; Benkovic, S. J. *Biochemistry* **1995**, *34*, 11037−11048.
(37) Gekko, K.; Yamagami, K.; Kunori, Y.; Ichihara, S.; Kodama, M.; Iwakura, M. *J. Biochem.* **1993**, *113*, 74−80.
(38) (a) Bajorath, J.; Li, Z.; Fitzgerald, G.; Kitson, D. H.; Farnum, M.; Fine, R. M.; Kraut, J.; Hagler, A. T. *Proteins: Struct., Funct., Genet.* **1991**, *11*, 263−270. (b) Bajorath, J.; Kraut, J.; Li, Z.; Kitson, D. H.; Hagler, A. T. *Proc. Natl. Acad. Sci. U.S.A.* **1991**, *88*, 6423−6426.
(39) Hehre, W. J.; Radom, L.; Schleyer, P. v.; Pople, J. A. *Ab Initio Molecular Orbital Theory*; Wiley-Interscience: New York, 1986.
(40) Benkovic, S. J.; Sammons, D.; Armarego, W. L. F.; Waring, P.; Inners, R. *J. Am. Chem. Soc.* **1985**, *107*, 3706−3712.

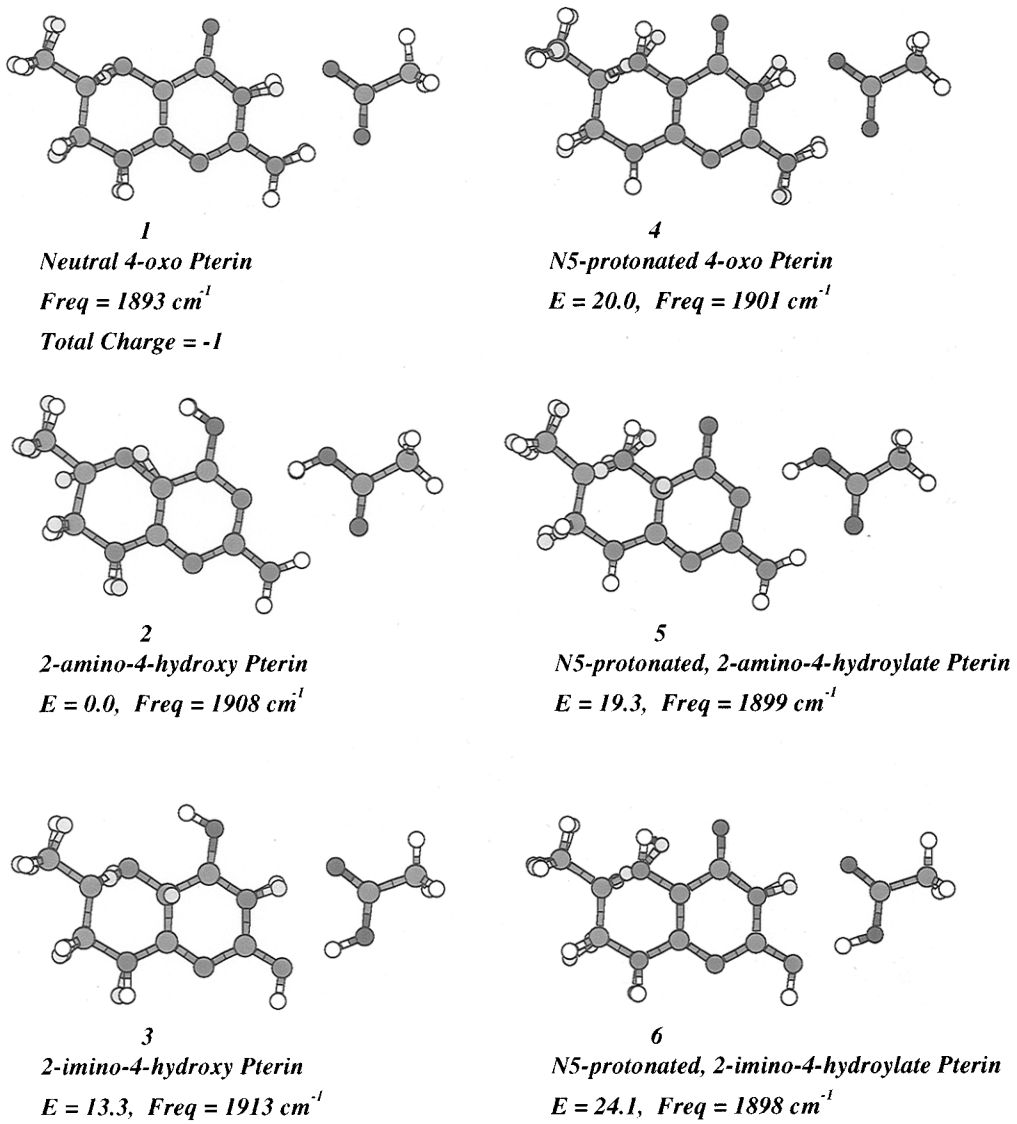

Figure 6. Minimum energy structures, normal mode displacements and characteristic frequencies, and relative energies of various acetic acid−pterin complexes employed as models of the DHFR active site complex.

vibrations for **5** and **6** are similar, but differ in frequency. The highest energy structure of the N5-protonated species is **6**, and not surprisingly this species contains an unusual vibration with a frequency of 2738 cm^{-1}, corresponding to a large displacement of the Asp 27 carboxyl hydrogen to well within bonding distance of the pterin N2. Thus, this vibration transforms **6** into **4** by transfer of a hydrogen across a soft potential energy surface (that is, the force constant for the carboxyl oxygen−carboxyl hydrogen is relatively weak). A similar process is indicated at a frequency of 2775 cm^{-1} for **4** in which the pterin N3 hydrogen is displaced to within bonding distance of the nearby Asp 27 carboxyl oxygen, resulting in transformation of this structure into **5** which is the low-energy structure for the N5-protonated series, and derives from the 4-hydroxy tautomer **2**. In vacuo, the N5-protonated structures are 19−24 kcal mol^{-1} less stable than the lowest energy 4-hydroxy structure.

Raman spectra for the region 1400−2000 cm^{-1} for **1**, **2**, and **4** are compared in Figure 7. As can be seen, vibrations of the N5−C6 bond for both **2** and **4** are at slightly higher energies than the same vibration in **1**, although **4** has a more intense Raman absorbance (∼750 Å/amu).

The implication of the vibrational frequencies determined by the electronic structure calculations is that a simple upward shift in Raman frequency for the N5−C6 stretch is not sufficient to demonstrate that N5 is the site of protonation. In vacuo, the relative energies of these structures favors the 4-hydroxy

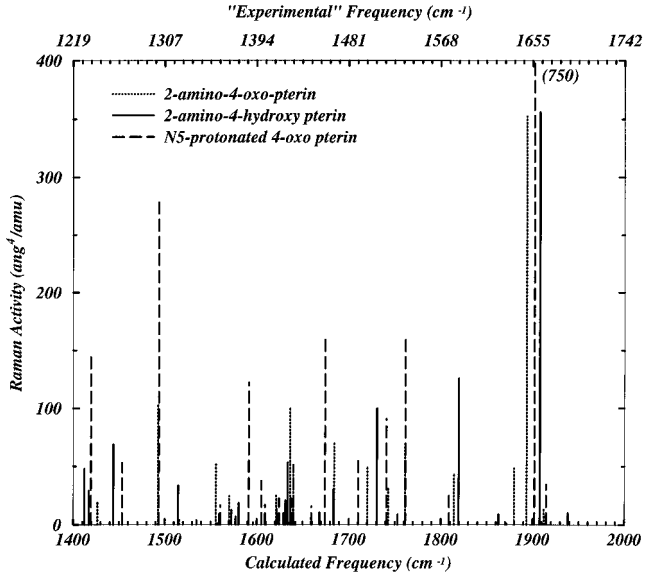

Figure 7. Calculated Raman spectra for structures **1**, **2**, and **4** from Figure 6 in the region of heavy atom vibrational frequencies.

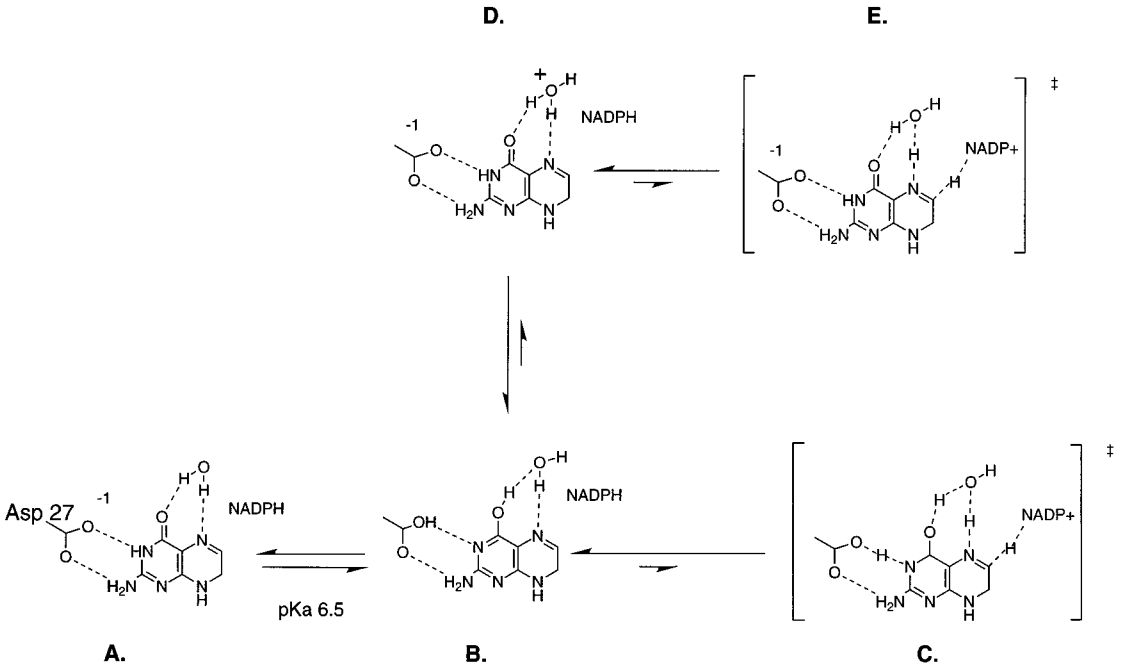

Figure 8. Catalytic mechanism which is consistent with both experimental data and the theoretical framework as determined by calculations.

tautomer of the pterin ring (**2**) binding to a neutral acetic acid. Of course, protein elements other than the side chain of Asp 27 must ultimately be taken into account, which we have done in this work with the use of classical electrostatic methods. Previous electronic structure calculations by Bajorath et al. found a buildup of electron density around the pterin O4, consistent with the results reported here.[38b]

An important question is whether such a reduced active site model is adequate for the examination of vibrational frequencies. In examining ligand binding, it is common now to implicitly include the electrostatic background due to charges on the enzyme instead of just a model side chain as done here. (In DHFR, Asp 27 is the only charged residue within 9.0 Å of the pterin ring, with all other nearby residues being neutral polar or nonpolar species.) Although the nonlocal charge background of an enzyme may moderate the binding energy to a ligand, vibrational frequencies are due to chemical bond forces which are much greater than the forces involved in nonbonded interactions. As such, vibrational frequencies, and particularly the relative ordering of these frequencies, are not expected to be significantly perturbed by the nonlocal charge background. In several crystallographic structures, however, a water molecule is found adjacent to the pterin O4 and N5 atoms.[12b,c] We plan to investigate the effects of this water in the future.

Relative Stability of the Pterin Tautomers. Quantum chemical calculations at the HF/6-31G level indicate that the 4-oxopterin is more stable than the 4-hydroxypterin by 0.2 kcal mol^{-1} *in vacuo*, but with such a small difference in heat of formation the relative stability of each in solution will be roughly determined by their dipole moments. In this case, the 4-oxopterin which has a dipole moment of 7.0 D, as determined by the quantum chemical calculations, will be favored over the 4-hydroxypterin which has a similarly determined dipole moment of 5.6 D. Which species is bound to the enzyme may vary with the degree of hydration of the active site and pH as discussed below. However, the hydride transfer step in *E. coli* DHFR has been shown to have a pK_a dependence of 6.5,[1] and the calculations indicate that only the 4-hydroxy ternary complex is capable of both an upward shift in pK_a and a vibrational perturbation of the N5−C6 bond to a higher frequency.

Implications for Catalysis

Conformational Changes Associated with Catalysis. The large pK_a shift for His 45 suggested that DHFR from other species may have similarly acting residues. Indeed, an alignment of 44 DHFR sequences from various species indicated that 34 of these enzymes contained weak bases at both of the positions corresponding to Arg 44 and His 45. In this regard, basic residues at position 45 likely play a more significant role than previously thought.

Previous determination of the electrostatic field around DHFR implied that Arg 44, Lys 76, and Arg 98 provided a structural motif that was important in polarizing the cofactor for catalysis.[38] However, the sequence alignment of the 44 DHFR enzymes indicated that only 5 of 44 sequences contained a weak base at position 98, although 18 of the 44 contained a weak base at position 101 (*E. coli* numbering), which may be structurally homologous to residue 98 of the *E. coli* enzyme. Similarly, 20 out of 44 of the sequences contained a weak base at position 75, 76, or 77 which would correspond to Lys 76 of the *E. coli* enzyme.

In all crystallographic structures examined so far, binding of cofactor, substrate, or inhibitor alters the pK_a of His 45. The effect of modifying His 45 has been examined for the *E. coli* enzyme[41,42] in which it was found that mutation to Asn decreases cofactor binding by more than 1 kcal mol^{-1}; however, the pH dependence of the E_1 and E_2 equilibria of the apoenzyme was not examined. Binding of the cofactor to the wild-type enzyme results in the presence of only one enzyme conformer,[2] and suggestively, the titration behavior of His 45 in the apoenzyme parallels the pH dependence of cofactor binding to the apoenzyme.[3]

Hydride Transfer. The mechanism that is consistent with both the electrostatic and quantum chemical calculations and the Raman study of DHFR complexes is shown in Figure 8. This mechanism differs from previously proposed mechanisms involving 4-hydroxy tautomers in that Asp 27 does not serve

(41) Chen, J. T.; Mayer, R. J.; Fierke, C. A.; Benkovic, S. J. *J. Cell. Biochem.* **1985**, *29*, 73−82.
(42) Adams, J.; Johnson, K.; Mathews, R.; Benkovic, S. J. *Biochemistry* **1989**, *28*, 6611−6618.

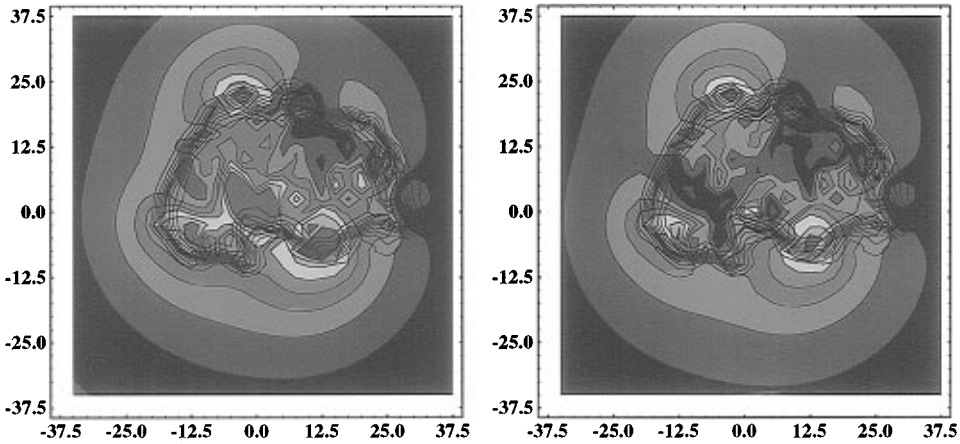

Figure 9. A slice through the electrostatic potential of the ternary complex of DHFR coincident with the plane of the pterin ring: left, ternary complex at pH 7.0 with Asp 27 ionized and binding the 4-oxopterin ring; right, ternary complex at pH 6.0 with Asp 27 protonated and binding the 4-hydroxypterin ring. The axes denote distances in units of 2.5 Å.

to donate a proton to form the 4-hydroxypterin. The initially bound pterin in Figure 8A exists in the 4-oxo tautomer and binds to the carboxylate group of Asp 27 by a dipole−charge interaction. Protonation of the pterin O4 occurs *via* solvent and is coupled with electronic rearrangement, resulting in movement of the pterin N3 proton onto the carboxylate of Asp 27 (Figure 8B).

Concerted with hydride transfer from the nicotinamide C4 to C6 of the pterin is movement of the pterin O4 proton onto N5, likely through a bound water molecule as shown in Figure 8C, and retransfer of the proton on Asp 27 back to the pterin N3. The product complex thus involves binding of the 4-oxo tautomer of H_4F to the Asp 27 carboxylate and re-formation of an unfavorable buried charge in the active site pocket, which may explain why the off rate for the product H_4F is higher above pH 6.2.[43]

Previous NMR studies with human DHFR have ruled out the existence of the 4-hydroxy tautomer of either H_2F or folate in the binary H_2F−DHFR complex, but did not examine the ternary complex used here.[44] The active site of the binary complex is fairly well solvated relative to the ternary complex, and so the 4-hydroxy tautomer may not form readily. This is in agreement with the Raman study, where perturbation of the N5−C6 vibration was not observed for the binary complex. NMR studies of folate in ternary complexes with *L. casei* DHFR indicate that folate does exist, at least partially, in the 4-hydroxy form.[45] NMR studies with the ternary complex of the *E. coli* enzyme have resulted in chemical shifts which are consistent with changes in the hybridization of the pterin ring[4] as would be expected for tautomerization from the 4-oxo- to the 4-hydroxypterin ring. These latter results, however, are inconsistent with N5 protonation as the chemical shift is in the wrong direction, as shown in previous studies.[46]

Driving Force for Reaction. If Asp 27 exists as a carboxylate in the unbound enzyme, burial of the charged side chain upon ligand binding is capable of providing a driving force for tautomerization. In the unliganded enzyme Asp 27 is exposed to solvent, and thus the charge exists in a relatively higher dielectric medium. However, substrate binding excludes solvent from the active site cavity and hence also reduces the local dielectric response. The buried charge of Asp 27 now exists in a low-dielectric region, as shown in the electrostatic potential map of the ternary enzyme complex involving the 4-oxopterin in Figure 9. The map represents the electrostatic potential of the active site at pH 7.0 taken through a plane coincident with the plane of the pterin ring. The axes measure distances in units of 2.5 Å with the plot centered near the carboxylate group of Asp 27. The protein/solvent or dielectric boundary is marked by the black gradations, which approximately represent the change from a dielectric constant of 20 to one of 80. Regions of high negative electrostatic potential are shown in red and change to relatively high positive potential as the colors change down the spectrum from red to violet (the complex has an overall charge of −12 at pH 7.0). As can be seen, most of the large changes in potential occur on the dielectric boundary, which corresponds to charge groups being located on the surface of the protein. A large area of high negative electrostatic potential, however, is seen to be located in the protein interior, centered near position 0, 0. This is the location of Asp 27.

The work required to move a charge from a high-dielectric environment to a low-dielectric environment can be as high as 20−50 kcal mol^{-1}.[47,48] The work required in any specific case will depend on the shape of the dielectric boundary and how deeply the charge is buried. Thus, it is more favorable to protonate Asp 27 as the dielectric boundary changes upon substrate binding rather than simply burying the charge. This is affected in an efficient manner by transfer of the pterin N3 hydrogen and protonation of O4, resulting in tautomerization of the bound substrate. The potential map for the resulting complex is also shown in Figure 9, where it can be seen that the interior of the protein is much more uniform in potential, with all large changes occurring on the protein surface. Because electrostatic potentials are additive, reducing the potential at Asp 27 by protonation also results in reductions elsewhere, as exemplified by the difference in potential around position 12.5, −7.5 between the two potential maps.

Thus, an important aspect of a proton shuffle mechanism for DHFR is the critical nature of the dielectric environment of the active site, the structure of which is shown in Figure 4. If the reactive centers are too close to the dielectric boundary between the protein interior and solvent, there will be an insufficient driving force for tautomerization of the pterin ring. The same dielectric boundary will effect binding of inhibitors such as

(43) Appleman, J. R.; Tsay, J. T.; Freisheim, J. H.; Blakely, R. L. *Biochemistry* **1992**, *31*, 3709−3715.
(44) Blakely, R. L.; Appleman, J. R.; Freisheim, J. H.; Jablonsky, M. J. *Arch,. Biochem. Biophys.* **1993**, *306*, 501−509.
(45) Cheung, H.; Birdsall, B.; Frenkiel, T. A.; Chau, D. D.; Feeney, J. *Biochemistry* **1993**, *32*, 6846−6854.
(46) Selinsky, B. S.; Perlman, M. E.; London, R. E.; Unkefer, C. J.; Mitchell, J.; Blakely, R. L. *Biochemistry* **1990**, *29*, 1290−1296.
(47) Gilson, M. K.; Rashin, A.; Fine, R.; Honig, B. *J. Mol. Biol.* **1985**, *183*, 503−516.
(48) Gilson, M. K.; Honig, B. H. *Proteins: Struct. Funct., Genet.* **1988**, *4*, 7−18.

methotrexate, as a low-dielectric environment will decrease the stability of the MTX−protein salt bridge.[26] Increasing the solvent accessibility or stabilizing charges in the active site by substitution of the active site hydrophobic residues shown in Figure 4 for smaller or more polar residues should affect the nature of substrate binding and decrease hydride-transfer rates. These trends are indeed observed experimentally. Substitution of Leu 28 in the active site of the *E. coli* enzyme (Figure 4) with Phe decreases the dielectric response, and experimentally it is observed that the hydride-transfer rate increases from 950 to 4000 s^{-1}.[49] Likewise, the wild-type human enzyme contains Phe at the analogous position (31), and when this residue is replaced with Leu, it is observed that the off rate for product release significantly decreases,[43] likely due to the increased local dielectric response and resulting stabilization of the charge−dipole interaction of Asp 27 with H_4F.

If formation of a low-dielectric environment around the Asp 27−pterin interaction is obligatory for catalysis, however, then an isomerization of the ternary complex such that water is relatively excluded from the active site along with movement of hydrophobic residues such as Leu 28 into proximity with Asp 27 might be expected prior to hydride transfer. It is likely that such events would also be concomitant with tautomerization of the pterin ring from the initially bound 2-amino-4-oxopterin (Figure 6, **1**) to the 2-amino-4-hydroxypterin (Figure 6, **2**). A hydrogen bond between Asp 27 and the amide of the pterin N3 with a barrier for proton transfer between the two heavy atoms which is lower than the barrier for hydride transfer would affect the nature of the transition state. In this regard, the synergistic effect of a charge−dipole interaction in which the H-bond length is relatively short coupled with the thermodynamic driving force of the removal of the buried charge may significantly reduce the barrier for proton transfer between N3 and Asp 27. This proton transfer would be concomitant with the protonation/tautomerization of the pterin O4. Furthermore, if the barrier for hydride transfer is intrinsically higher than that for the proton shuffling as described here, then the proton shuffling may occur relatively frequently compared to movement of the hydride ion.

In this respect, it is worthwhile to consider the mechanism and isomerization within the framework outlined by Northrup and McCammon for reactions involving high dimensionality.[50] In such a scheme, the pathway in Figure 8, B → D, in which a proton effectively oscillates between the Asp 27 carboxyl and a crystallographically observed water, may be kinetically more favorable. Protonation of Asp 27 serves to localize the proton near the reactive center (A → B), and the barrier to products is surmounted by traversing through the intermediate state of Figure 8D and on to a lower energy transition state species, E, of Figure 8, rather than directly over the barrier from the ground state of B to the transition state structure depicted in Figure 8C.

For this case, the mechanism depicted in Figure 8, B → D, suggests that solvent isotope effects would be somewhat masked, depending on how much higher the barrier for hydride transfer is relative to proton transfer. Furthermore, as determination of the rate of proton transfer from Asp 27 to the water interacting with the pterin N5 is dependent on protonation of Asp 27, the rate of the active site isomerization may also depend on pH.

Such kinetic phenomena have been implied in the study of DHFR from various species by analyzing isotope effects in the pre-steady-state burst reaction.[51] In mammalian enzymes the pre-steady-state kinetics are limited by the rate of an obligatory isomerization of the reactive complex, after which hydride transfer occurs rapidly from NADPH to H_2F. The same obligatory isomerization was also implicated for bacterial enzymes; however, in this case analysis of the isotope effects demonstrated that the hydride-transfer step is rate limiting, except at pH 5.0 in which case an isomerization becomes the rate-limiting step.

Conclusion

When a low-dielectric response of the protein interior is examined in the Poisson−Boltzmann calculations, the only titrating group that is consistent with a pK_a of 6.5 is a protonation/tautomerization of the pterin ring of H_2F to the 4-hydroxypterin. These results are consistent with the quantum chemical calculations which examine the relative energies and vibrational frequencies of several active site tautomers. The mechanism that is consistent with both experimental results[1,4,13] and the calculations presented here involves formation of the 4-hydroxypterin in the active site of DHFR, as shown in Figure 8. The driving force for the tautomerization step is the change in the dielectric environment of the substrate and active site when the substrate binds, resulting in the burial of a charge in a low-dielectric environment. The change in the dielectric response of the environment shifts the pK_a of Asp 27 upward, and results in protonation of Asp 27 and formation of the 4-hydroxy form of the pterin ring of the substrate, which is then poised for the chemical reaction. This titration−tautomerization step serves to localize a proton in the active site of the reactive complex, from which hydride transfer follows.

More generally, DHFR catalyzes the reaction by providing an architecture which complements the reaction and allows it to proceed under favorable conditions: the reactants are brought within close proximity and aligned with respect to each other by binding, the low-dielectric environment of the active site induces an electronic reorganization of the reactants by rearrangement of protons such that they are preorganized to an optimal configuration for catalysis, and finally the enzyme provides an appropriate reaction field or environmental background for the chemical transformation.[38b]

Acknowledgment. We thank J. A. McCammon for kindly providing the UHBD program, J. Antosiewicz for technical assistance in the early stages of this work, and B. Honig for suggestions while this work was in progress. This work was supported by Grants NIH GM24129 (S.J.B.) and NSF CHE-9317429 (B.J.G.). W.R.C. is a recipient of an NIH postdoctoral fellowship.

Note Added in Proof. Subsequent to the completion of this work, crystallographic evidence was presented for the existence of the 4-hydroxy tautomer of H_2F bound to *E. coli* DHFR (Lee, H.; Reyes, V. M.; Kraut, J.; *Biochemistry* **1996**, *35*, 7012−7020).

Supporting Information Available: A listing of pK_a values for all protein residues (1 page). See any current masthead page for ordering and Internet access instructions.

JA962621R

(49) Wagner, C. R.; Thillet, J.; Benkovic, S. J. *Biochemistry* **1992**, *31*, 7834−7840.
(50) Northrup, S. H.; McCammon, J. A. *J. Am. Chem. Soc.* **1984**, *106*, 930−934.
(51) Beard, W. A.; Appleman, J. R.; Delcamp, T. J.; Feisheim, J. H.; Blakely, R. L. *J. Biol. Chem.* **1989**, *264*, 9391−9399.
(52) Saenger, W. *Principles of Nucleic Acid Structure*; Springer-Verlag: New York, 1984.
(53) Maharaj, G.; Selinsky, B. S.; Appleman, J. R.; Perlman, M.; London, R. E.; Blakely, R. L. *Biochemistry* **1990**, *29*, 4554−4560.
(54) Poe, M. *J. Biol. Chem.* **1977**, *252*, 3724−3728.